Supplement of Atmos. Chem. Phys., 26, 11771–11784, 2026
https://doi.org/10.5194/acp-26-11771-2026-supplement

Atmospheric Chemistry and Physics
Open Access

Supplement of

Measurement report: Dust Transport and Local Anthropogenic Emissions Differently Shape Atmospheric Ice-Nucleating Particles in an Industrial Urban Atmosphere

Jiawei Yang et al.

Correspondence to: Zhijun Wu (zhijunwu@pku.edu.cn)

S1. Supplementary Tables

Table S1. The Pearson correlation coefficients between pollutants and the measured N_{INP} at different temperatures are presented, with significant results at the 95% confidence level ($p < 0.05$) highlighted in bold. "HM" is the sum of 8 $PM_{2.5}$-bound heavy metals (Cd, Cr, Hg, As, Pb, Cu, Zn, Ni). $N_{>0.5μm}$, $N_{<1μm}$, and $N_{>1μm}$ refer to the particle number concentrations with diameters larger than 0.5 μm, smaller than 1 μm, and larger than 1 μm, respectively.

Factors	−10 °C	−12.5 °C	−15 °C	−17.5 °C	−20 °C
Fe	0.22	0.13	0.14	0.05	-0.20
K	-0.01	0.17	0.02	-0.11	-0.06
Ca	**0.44**	0.27	0.33	0.33	0.08
Zn	0.12	0.16	0.14	-0.02	-0.19
Pb	0.32	0.38	0.34	0.29	0.10
Mn	0.10	0.09	0.13	-0.01	-0.28
Cu	-0.03	0.15	0.01	-0.10	-0.07
As	0.17	0.11	0.11	-0.01	-0.12
Ag	-0.04	-0.12	-0.08	-0.03	0.27
Ga	0.11	0.11	0.14	-0.03	-0.05
Cr	-0.03	-0.09	-0.12	-0.21	-0.39
Se	0.12	0.10	0.08	-0.11	-0.12
Co	**0.61**	**0.61**	**0.45**	0.38	0.22
Sr	-0.03	0.15	0.00	-0.12	-0.05
Cd	-0.06	-0.05	0.00	0.02	0.03
Ba	-0.02	0.15	0.00	-0.10	-0.05
Hg	0.12	0.19	0.16	-0.09	-0.19
Ni	-0.12	-0.18	-0.09	-0.25	**-0.41**
Au	**-0.49**	**-0.50**	**-0.44**	-0.27	-0.07
NO_3^-	0.06	-0.03	-0.02	-0.16	-0.18
SO_4^{2-}	0.04	-0.01	-0.02	-0.20	-0.17
NH_4^+	0.07	0.00	0.00	-0.17	-0.19
Cl^-	0.11	0.19	0.16	-0.06	-0.24
K^+	-0.01	0.16	0.02	-0.11	-0.08
Na^+	0.01	0.04	0.18	0.00	-0.34
Mg^{2+}	0.05	0.22	0.07	-0.06	-0.08
Ca^{2+}	0.22	0.23	0.30	0.33	-0.16
SO_2	-0.08	-0.03	0.10	0.05	-0.33
HNO_2	0.23	0.22	0.18	0.07	-0.08
HNO_3	0.17	0.09	0.09	-0.02	-0.04
NH_3	0.39	0.32	0.25	0.14	-0.01
HCl	-0.10	-0.03	0.03	-0.02	-0.25
OC	0.23	0.16	0.23	0.03	-0.13
EC	0.17	0.11	0.18	0.03	-0.18
PM_{10}	0.17	0.12	0.14	-0.02	-0.20
$PM_{2.5}$	0.11	0.08	0.07	-0.12	-0.18
HM	0.06	0.19	0.08	-0.07	-0.14
$N_{>0.5μm}$	-0.03	-0.06	-0.07	-0.15	-0.16
$N_{<1μm}$	-0.15	-0.15	-0.07	0.00	-0.33
$N_{>1μm}$	0.10	0.04	0.05	-0.01	-0.21

Table S2. Pearson correlation coefficients between daily mean PMF-resolved source contributions and N_{INP} at different temperatures during non-desert-dust periods. Values are shown as r (p value). Values indicating complete freezing before the corresponding temperature were excluded from the correlation analysis.

Aerosol source	−10 °C	−12.5 °C	−15 °C	−17.5 °C	−20 °C
Industry	−0.031 (0.886)	−0.148 (0.490)	−0.159 (0.459)	−0.126 (0.557)	−0.264 (0.274)
Dust related	0.313 (0.137)	0.180 (0.401)	0.220 (0.302)	0.265 (0.211)	0.209 (0.391)
Secondary aerosol	0.056 (0.794)	−0.014 (0.949)	−0.014 (0.949)	−0.066 (0.758)	0.145 (0.554)
Coal & Traffic	0.178 (0.406)	0.194 (0.364)	0.219 (0.305)	0.092 (0.668)	0.035 (0.886)
Fireworks	0.006 (0.978)	0.182 (0.396)	0.020 (0.928)	−0.088 (0.684)	0.108 (0.661)

Table S3. N_{INP} values and corresponding 95% confidence intervals at selected temperatures. Values are shown as N_{INP} (lower–upper), in units of L−1. n.q. = not quantified because complete freezing occurred before the corresponding temperature.

Sample date	−10 °C	−12.5 °C	−15 °C	−17.5 °C	−20 °C
2023/12/4	0.157 (0.0726–0.337)	0.354 (0.211–0.594)	0.902 (0.651–1.25)	3.53 (2.99–4.17)	11.8 (10.8–12.9)
2023/12/5	4.14 (3.52–4.88)	11.6 (10.5–12.8)	n.q.; 13.4 (12.2–14.6) at −13.0 °C	n.q.	n.q.
2023/12/6	1.08 (0.8–1.47)	3.51 (2.96–4.16)	6.24 (5.49–7.08)	12.3 (11.3–13.5)	n.q.
2023/12/7	1.15 (0.858–1.55)	3.36 (2.83–4)	4.91 (4.25–5.67)	12.4 (11.3–13.6)	n.q.
2023/12/8	1.19 (0.88–1.61)	4.34 (3.7–5.08)	6.72 (5.92–7.63)	n.q.	n.q.
2023/12/9	1.06 (0.758–1.48)	3.56 (2.97–4.27)	6.11 (5.31–7.02)	14.4 (13.2–15.8)	n.q.
2023/12/10	0.0907 (0.0282–0.29)	0.339 (0.181–0.635)	0.653 (0.414–1.03)	2.74 (2.19–3.42)	16.7 (15.3–18.3)
2023/12/11	0.0563 (0.00976–0.318)	0.171 (0.0585–0.498)	0.47 (0.241–0.913)	1.13 (0.729–1.74)	3.67 (2.88–4.67)
2023/12/12	0.0379 (0.00368–0.363)	0.31 (0.121–0.789)	0.47 (0.218–1.01)	1.33 (0.839–2.12)	3.81 (2.89–5.01)
2023/12/13	0 (0–0.146)	0.0962 (0.0299–0.308)	0.175 (0.0723–0.424)	0.297 (0.15–0.591)	n.q.
2023/12/14	0 (0–0.121)	0.0478 (0.011–0.206)	0.18 (0.0805–0.4)	0.927 (0.646–1.33)	n.q.
2023/12/17	0 (0–0.101)	0 (0–0.101)	0.0936 (0.0345–0.253)	0.645 (0.435–0.955)	3.94 (3.35–4.62)
2023/12/18	0.153 (0.0565–0.415)	0.679 (0.416–1.11)	1.35 (0.951–1.91)	4.37 (3.6–5.31)	15.8 (14.3–17.5)
2023/12/20	0.0129 (0.00125–0.123)	0.133 (0.0573–0.307)	0.288 (0.161–0.513)	0.883 (0.633–1.23)	6.48 (5.73–7.33)
2023/12/21	0.013 (0.00126–0.125)	0.0659 (0.0205–0.211)	0.276 (0.152–0.499)	2.08 (1.67–2.59)	n.q.
2023/12/22	0 (0–0.109)	0.0142 (0.00138–0.136)	0.399 (0.238–0.669)	1.15 (0.843–1.56)	3.6 (3.03–4.29)
2023/12/23	0.0929 (0.0342–0.252)	0.54 (0.352–0.827)	0.99 (0.721–1.36)	1.52 (1.18–1.97)	5.99 (5.26–6.82)
2023/12/24	0.0273 (0.00473–0.154)	0.319 (0.181–0.561)	1.51 (1.16–1.97)	3.13 (2.61–3.76)	7.62 (6.78–8.56)
2023/12/25	0.0284 (0.00492–0.16)	0.101 (0.0372–0.273)	0.237 (0.122–0.46)	0.808 (0.561–1.16)	2.55 (2.08–3.13)
2023/12/26	0 (0–0.102)	0.123 (0.0508–0.298)	0.47 (0.296–0.747)	1.21 (0.901–1.61)	3.5 (2.95–4.15)
2023/12/27	0.0656 (0.018–0.238)	0.254 (0.128–0.505)	0.437 (0.258–0.741)	1.81 (1.39–2.35)	5.05 (4.31–5.91)
2023/12/28	0.0618 (0.0142–0.266)	0.211 (0.0908–0.487)	0.551 (0.325–0.934)	1.2 (0.836–1.72)	4.11 (3.38–4.99)
2023/12/29	0 (0–0.269)	0.0351 (0.00341–0.336)	0.473 (0.226–0.989)	2.01 (1.39–2.89)	7.26 (5.99–8.8)
2023/12/30	0.103 (0.038–0.28)	0.243 (0.125–0.472)	0.424 (0.255–0.704)	1.19 (0.878–1.61)	7.81 (6.93–8.8)
2023/12/31	0 (0–0.101)	0.0132 (0.00128–0.126)	0.0532 (0.0146–0.193)	0.136 (0.0585–0.314)	2.38 (1.94–2.92)
2024/1/1	0.0221 (0.00214–0.211)	0.298 (0.142–0.623)	0.443 (0.241–0.814)	0.751 (0.469–1.2)	8.73 (7.59–10)
2024/1/2	0.134 (0.058–0.311)	0.784 (0.549–1.12)	1.27 (0.958–1.68)	2.36 (1.92–2.9)	7.64 (6.81–8.57)
2024/1/3	0.107 (0.0418–0.272)	0.428 (0.265–0.691)	0.782 (0.548–1.12)	n.q.	n.q.
2024/1/4	0.0943 (0.0347–0.255)	0.755 (0.524–1.09)	2.02 (1.61–2.52)	12.3 (11.3–13.5)	n.q.
2024/1/5	0.0395 (0.00907–0.17)	0.107 (0.0419–0.272)	0.263 (0.143–0.483)	0.954 (0.691–1.32)	3.92 (3.34–4.6)

S2. Supplementary Figures

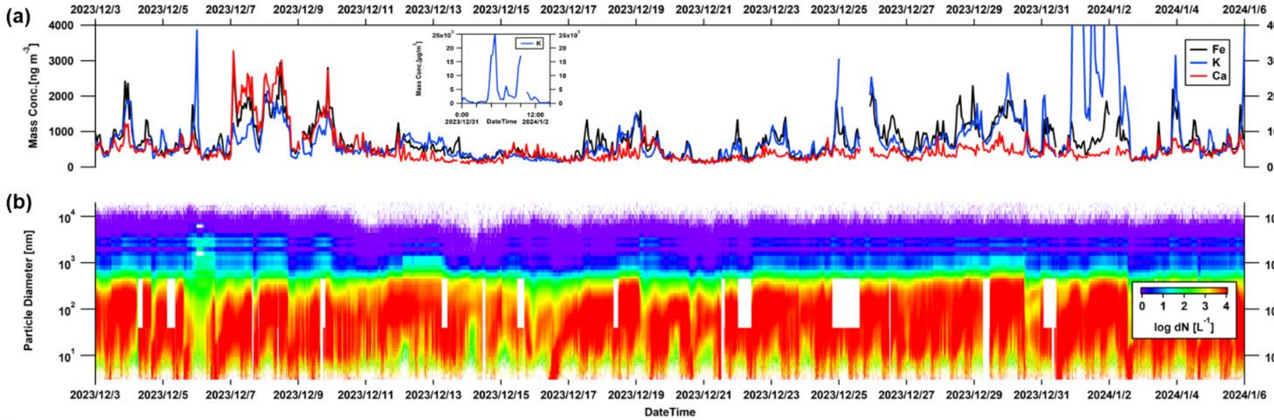

Figure S1. Time series of aerosol physicochemical parameters observed in Taiyuan from December 2023 to January 2024. (a) Mass concentrations of representative metallic elements (Fe, K, Ca) measured by XRF. (b) Particle number size distributions (PNSD) obtained from SMPS and OPC measurements.

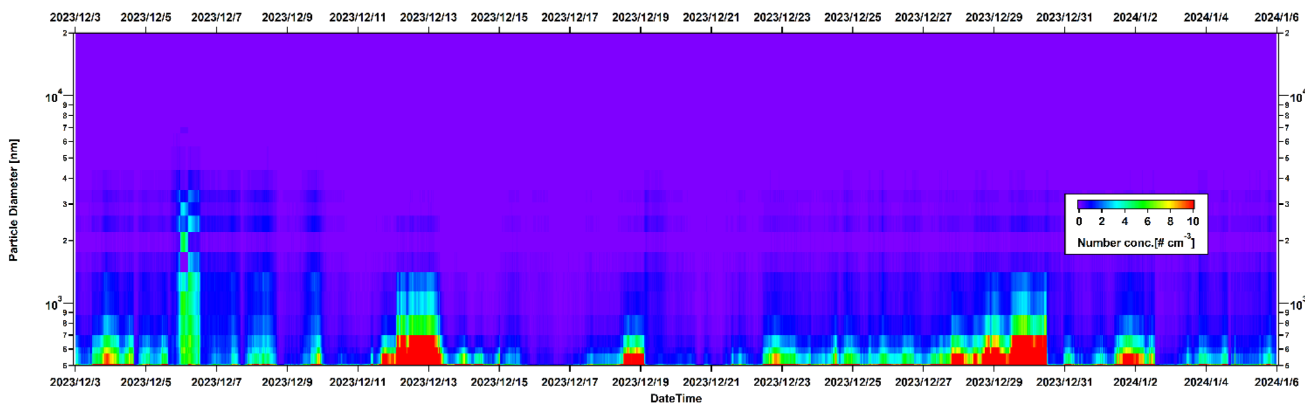

Figure S2. Particle number size distribution (PNSD) for particles larger than 500 nm.

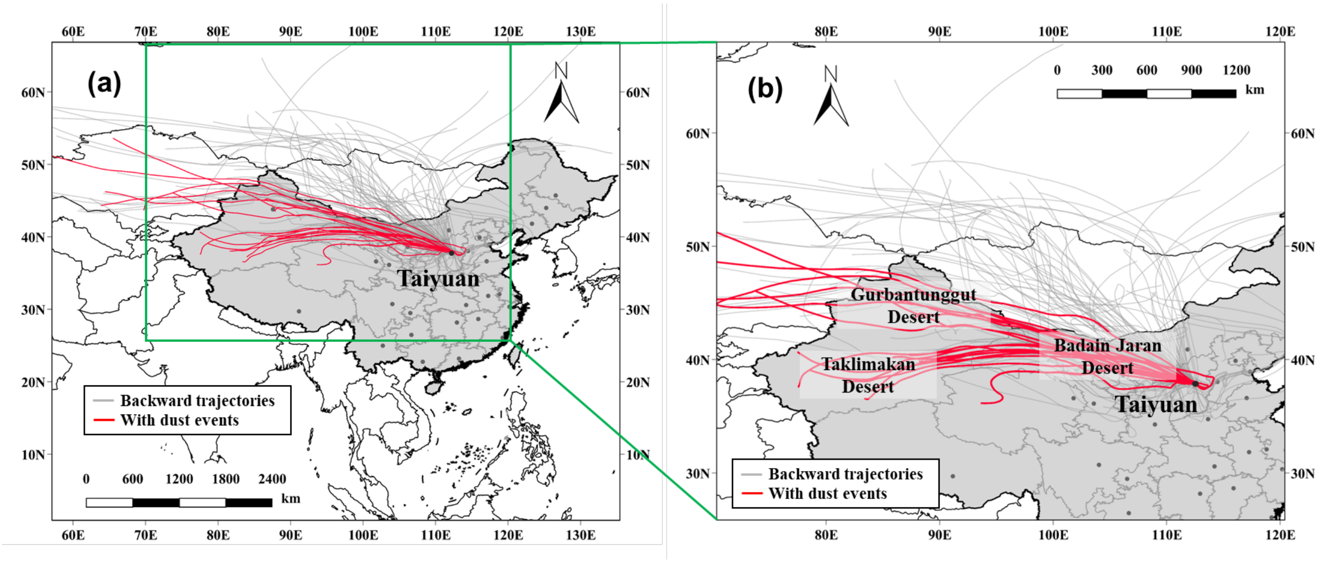

Figure S3. 72-hour backward trajectories of air masses at different scales. (a) All backward trajectories (in gray) during the observation period, along with the results of trajectory clustering. (b) Backward trajectories during the dust transport episode, highlighted in red, with the locations of the three major deserts in northwestern China indicated. The maps were generated by the authors using MeteoInfoMap (Wang, 2014).

Five factors were identified in the PMF analysis to resolve the sources and contributions of $PM_{2.5}$, with the resulting factor profiles and contributions shown in Fig. S4. Factor 1 showed high contributions of Cr and Mn, where Cr is mainly emitted from coal combustion and metallurgical industries such as steel production (Song and Gao, 2011), while Mn is associated with metal smelting and manufacturing processes (Zheng et al., 2014). Considering the developed metallurgical, chemical, and coal industries in Taiyuan (Tang et al., 2014), this factor was identified as industrial emissions. Factor 2 was dominated by Ca and Fe, both crustal elements closely related to dust and resuspended (soil) dust particles (Chen et al., 2024; Huy et al., 2020; Lin et al., 2015) and thus was attributed to dust-related sources. Factor 3 exhibited high loadings of SO_4^{2-}, NO_3^-, and Cl^-, with a moderate contribution from OC, and was interpreted as secondary aerosols, comprising both secondary inorganic and organic components (Hopke et al., 2020; Srivastava et al., 2021). Factor 4 was enriched in Zn, Pb, Mn, As, EC and OC. Zn and Mn are tracers for vehicle exhaust and brake or tire wear (Yatkin and Bayram, 2007); Pb has multiple origins, including vehicular emissions (Smichowski et al., 2007; Srivastava et al., 2021). EC, OC and As are all recognized tracers of coal combustion (Oros and Simoneit, 2000; Srivastava et al., 2021). Therefore, this factor was identified as a mixed source associated with coal combustion and traffic emissions. Factor 5 was characterized by high Cu, Ba and K loadings, elements commonly used as additives in fireworks to produce colored flames (Rocco et al., 2025). The elevated K levels likely originate from potassium salts which serve as common oxidizers in pyrotechnic formulations (Martín-Alberca and García-Ruiz, 2014). This factor was therefore identified as a fireworks-related source. The correlation heatmap (Fig. S5) also reveals strong correlations among certain species, such as Cu, Ba, and Sr (fireworks); Mn and Fe (industrial); and Zn and Pb (traffic), which may corroborate the source assignments.

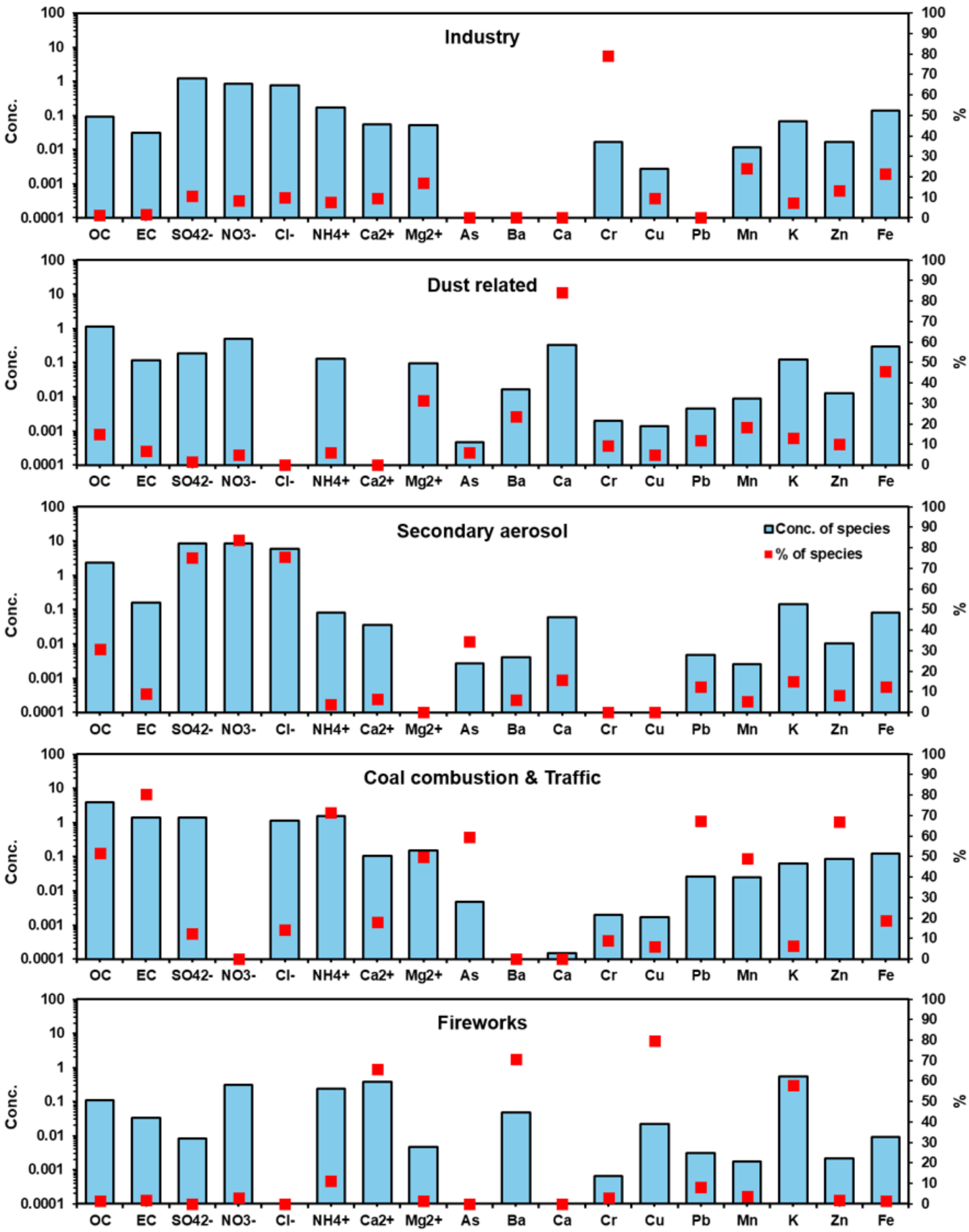

Figure S4. PMF factor profiles for ambient $PM_{2.5}$ in Taiyuan.

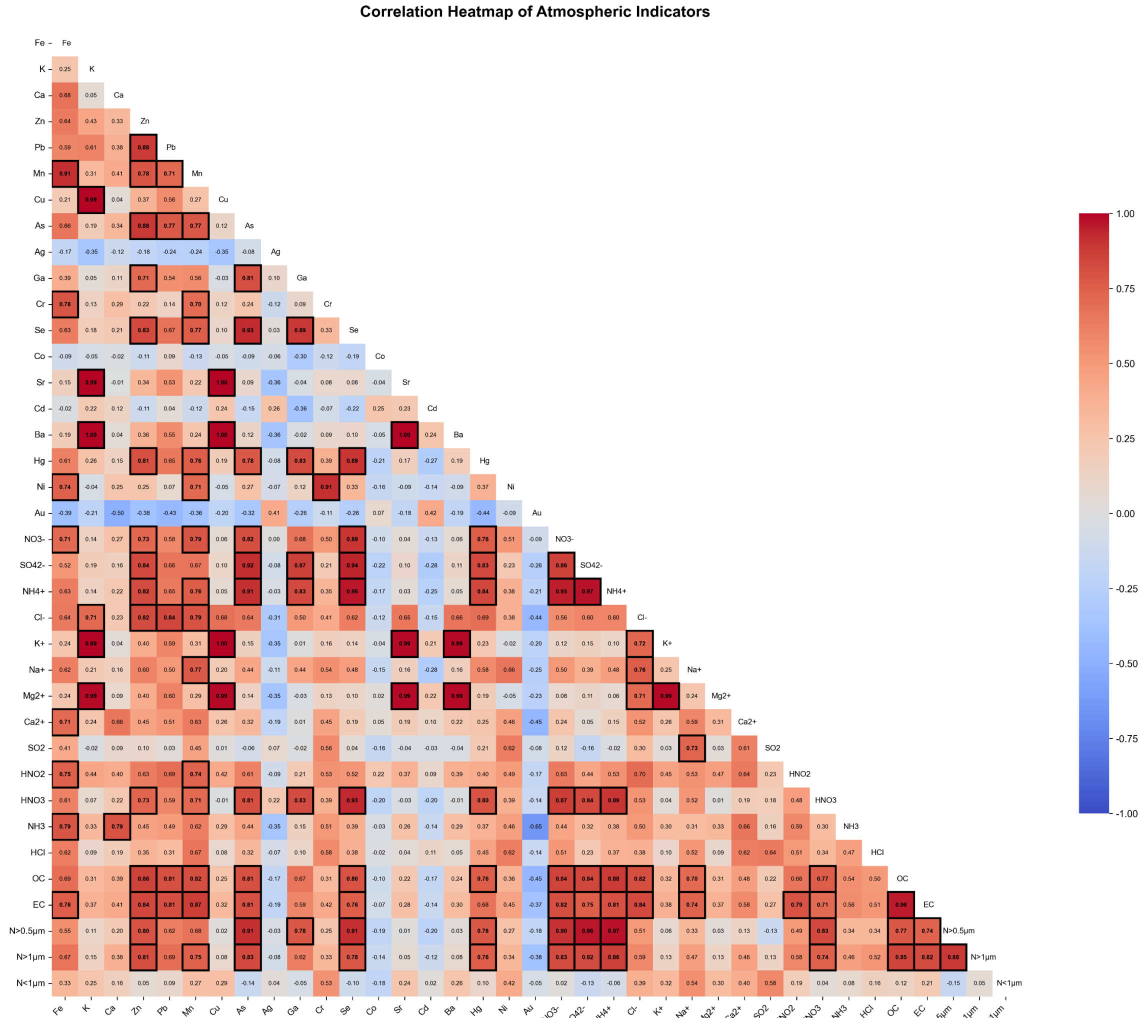

Figure S5. Heatmap of correlation analysis for various atmospheric species. Correlation coefficients (R) are indicated numerically and by color (sample size n = 25).

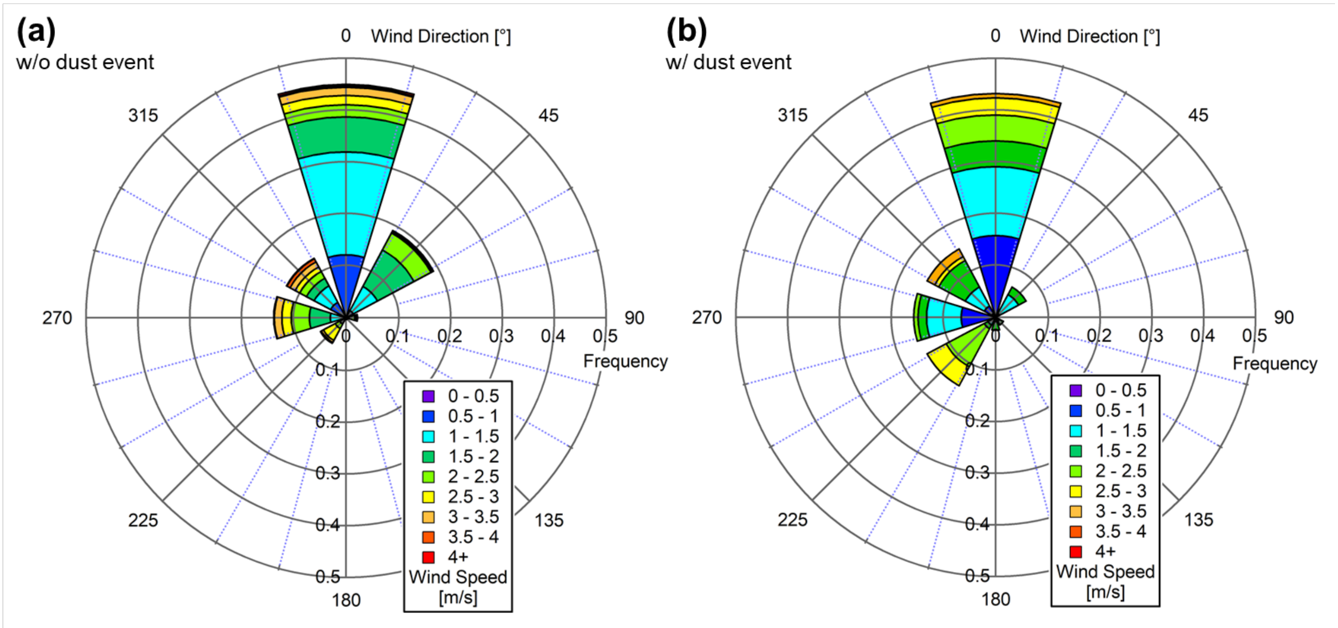

Figure S6. Wind rose plots for (a) the non-desert-dust periods and (b) the identified desert dust event during the campaign. Both periods were dominated by northerly flow, while the dust-event period showed a more concentrated northerly flow pattern. The plots are included to provide supplementary meteorological context for the event classification.

References

Chen, J., Wu, Z., Gong, X., Qiu, Y., Chen, S., Zeng, L., and Hu, M.: Anthropogenic Dust as a Significant Source of Ice-Nucleating Particles in the Urban Environment, Earth's Future, 12, e2023EF003738, https://doi.org/10.1029/2023EF003738, 2024.

Hopke, P. K., Dai, Q., Li, L., and Feng, Y.: Global review of recent source apportionments for airborne particulate matter, Science of The Total Environment, 740, 140091, https://doi.org/10.1016/j.scitotenv.2020.140091, 2020.

Huy, D. H., Thanh, L. T., Hien, T. T., and Takenaka, N.: Comparative study on water-soluble inorganic ions in PM2.5 from two distinct climate regions and air quality, Journal of Environmental Sciences, 88, 349–360, https://doi.org/10.1016/j.jes.2019.09.010, 2020.

Lin, Y.-C., Tsai, C.-J., Wu, Y.-C., Zhang, R., Chi, K.-H., Huang, Y.-T., Lin, S.-H., and Hsu, S.-C.: Characteristics of trace metals in traffic-derived particles in Hsuehshan Tunnel, Taiwan: size distribution, potential source, and fingerprinting metal ratio, Atmospheric Chemistry and Physics, 15, 4117–4130, https://doi.org/10.5194/acp-15-4117-2015, 2015.

Martín-Alberca, C. and García-Ruiz, C.: Analytical techniques for the analysis of consumer fireworks, TrAC Trends in Analytical Chemistry, 56, 27–36, https://doi.org/10.1016/j.trac.2013.12.010, 2014.

Oros, D. R. and Simoneit, B. R. T.: Identification and emission rates of molecular tracers in coal smoke particulate matter, Fuel, 79, 515–536, https://doi.org/10.1016/S0016-2361(99)00153-2, 2000.

Rocco, D., Morales, E., Deflin, T., Truong, J., Ju, J., and Curtis, D. B.: The Impact of Fireworks on Selected Ambient Particulate Metal Concentrations Associated with the Independence Day Holiday, Atmosphere, 16, 17, https://doi.org/10.3390/atmos16010017, 2025.

Smichowski, P., Gómez, D., Frazzoli, C., and Caroli, S.: Traffic-Related Elements in Airborne Particulate Matter, Applied Spectroscopy Reviews, 43, 23–49, https://doi.org/10.1080/05704920701645886, 2007.

Song, F. and Gao, Y.: Size distributions of trace elements associated with ambient particular matter in the affinity of a major highway in the New Jersey–New York metropolitan area, Atmospheric Environment, 45, 6714–6723, https://doi.org/10.1016/j.atmosenv.2011.08.031, 2011.

Srivastava, D., Xu, J., Vu, T. V., Liu, D., Li, L., Fu, P., Hou, S., Moreno Palmerola, N., Shi, Z., and Harrison, R. M.: Insight into $PM_{2.5}$ sources by applying positive matrix factorization (PMF) at urban and rural sites of Beijing, Atmospheric Chemistry and Physics, 21, 14703–14724, https://doi.org/10.5194/acp-21-14703-2021, 2021.

Tang, D., Wang, C., Nie, J., Chen, R., Niu, Q., Kan, H., Chen, B., and Perera, F.: Health benefits of improving air quality in Taiyuan, China, Environment International, 73, 235–242, https://doi.org/10.1016/j.envint.2014.07.016, 2014.

Wang, Y. Q.: MeteoInfo: GIS software for meteorological data visualization and analysis, Meteorological Applications, 21, 360–368, https://doi.org/10.1002/met.1345, 2014.

Yatkin, S. and Bayram, A.: Elemental composition and sources of particulate matter in the ambient air of a Metropolitan City, Atmospheric Research, 85, 126–139, https://doi.org/10.1016/j.atmosres.2006.12.002, 2007.

Zheng, M., Zhang, Y., Yan, C., Zhu, X., Schauer, J. J., and Zhang, Y.: Review of PM2.5 Source Apportionment Methods in China, Acta Scientiarum Naturalium Universitatis Pekinensis, 50, 1141–1154, https://doi.org/10.13209/j.0479-8023.2014.068, 2014.